ANL/OEPM-80-1

ANL/OEPM-80-1

GALVANOSTATIC POLARIZATION OF ZINC MICROANODES IN KOH ELECTROLYTES

by

Ming-Biann Liu, G. M. Cook,
and N. P. Yao

ARGONNE NATIONAL LABORATORY, ARGONNE, ILLINOIS

Prepared for the U. S. DEPARTMENT OF ENERGY
under Contract W-31-109-Eng-38

DISCLAIMER

Printed in the United States of America
Available from
National Technical Information Service
U. S. Department of Commerce
5285 Port Royal Road
Springfield, VA 22161

NTIS price codes
Printed copy: A03
Microfiche copy: A01

Distribution Category:
Energy Storage--Electrochemical-
Nearterm Batteries (UC-94ca)

ANL/OEPM-80-1

ARGONNE NATIONAL LABORATORY
9700 South Cass Avenue
Argonne, Illinois 60439

GALVANOSTATIC POLARIZATION OF ZINC MICROANODES IN KOH ELECTROLYTES

by

Ming-Biann Liu, G. M. Cook, and N. P. Yao

Chemical Engineering Division

May 1980

THIS PAGE

WAS INTENTIONALLY

LEFT BLANK

TABLE OF CONTENTS

LIST OF FIGURES

LIST OF TABLES

GALVANOSTATIC POLARIZATION OF ZINC MICRO-ANODES IN KOH ELECTROLYTES

by

Ming-Biann Liu, G. M. Cook, and N. P. Yao

ABSTRACT

This report includes a critical review of the current literature on the anodic passivation of zinc electrodes, a description of supplementary experimental studies to extend the data to a low current density region and to provide a basis for evaluating conflicting results of published work, and a new interpretation of the anodic passivation mechanism. This work provides a starting point for understanding passivation phenomena in battery electrodes.

The utilization of a zinc electrode in alkaline batteries depends on the ability of the electrode to remain active during the anodic dissolution process. This dissolution period is often terminated by the onset of passivation. Previous researchers have typically correlated the current density, i, and the passivation time, t, by the equation $(i - i_e)t^{1/2} = k$, where i_e corresponds to diffusion-excluded convective current density, and k is the correlation constant. Their investigations of passivation show that the values of i_e and k depend on experimental conditions such as electrode orientation.

We conducted further experiments on the effects of current density on passivation time of a small zinc anode (6.6×10^{-3} cm^2) in KOH at concentrations of 0.784, 2.92, 4.98 and 7.24M KOH as well as 7.24M KOH saturated with zinc oxide. We have concluded that there are two mechanisms for anodic passivation, one occurring at current densities below about 150 mA/cm^2 and another at higher current densities. Accordingly, in the overall mechanism, the total time to passivation includes the times to achieve the maximum zincate concentration as well as to form porous type I ZnO and compact type II ZnO.

In Ni/Zn batteries under development for vehicle propulsion, the electrolyte is usually 30% KOH (7M) saturated with zinc oxide; and the zinc electrode is formed in-situ by electro-deposition of zinc onto the grid. Using the data from our tests, we were able to estimate the effect of passivation on the utilization of the zinc electrode in an alkaline battery. For our calculations, we assumed a current density of 20 mA/cm^2 for a Ni/Zn battery cycled at 2-h rate. Based on a knowledge of the structure of zinc electrodeposits, we estimated that the zinc electrode has a porosity of 0.6 at the fully charged state. Using data available in the literature and our own data, we calculated a current density of 338 mA/cm^2 to be that above which the passivation limits the utilization of the zinc electrode.

I. INTRODUCTION

Alkaline batteries employing zinc electrodes are under development for use as near-term batteries for electric vehicles. Knowledge of the electrode behavior in KOH electrolyte is an important aspect of this development effort.

The utilization of a zinc electrode in alkaline batteries depends on the ability of the electrode to remain active in the anodic dissolution process:

$$Zn + 4OH^- \longrightarrow Zn(OH)_4^{2-} + 2e \qquad (1)$$

At anodic potentials near the equilibrium value, the oxidation product of zinc in concentrated alkaline solutions is $Zn(OH)_4^{2-}$ as evidenced by NMR (nuclear magnetic resonance) studies[1-3] as well as Raman and infrared reflection spectral study.[2] Many workers[4-14] have made galvanostatic measurements of planar zinc electrodes in alkaline solution; a general feature of the termination of the active dissolution period was found to be the onset of passivation with a sudden change toward positive potentials and oxygen evolution. Hampson et al.[15,16] observed that the transition of a porous electrode from an active to a passive condition was not so abrupt as that for a planar zinc electrode, and was accompanied by a gradual increase in electrode potential corresponding to the penetration of the reaction into the depth of the anode as pore surfaces became blocked or passivated with oxide.

Three different mechanisms have been proposed to explain zinc passivation behavior in alkaline solutions, namely, dissolution-precipitation, adsorption, and nucleation and two-dimensional growth of crystals. In the dissolution-precipitation model,[11,13,17,18] zincate builds up in the solution layer in the vicinity of the electrode surface as dissolution proceeds until the concentration reaches a critical value corresponding to the "solubility" of zinc in the solution. At this point, the precipitation of ZnO or $Zn(OH)_2$ occurs and subsequently retards the dissolution of zinc. This latter effect results in a rapid rise in potential until oxygen evolution begins. In the adsorption model,[19,20] hydroxide is adsorbed by the zinc electrode to form a monolayer of $Zn(OH)_2$, which releases protons to form a passive zinc-oxide film, thereby retarding the diffusion of hydroxide ion. When the diffusion rate of hydroxide ions is not sufficient to support the anodic current, passivation occurs. In the nucleation and crystal growth model,[21,22] zinc oxide nuclei form on the surface, and passivation occurs when the surface is inactivated by a full coverage of ZnO monolayer.

In all three mechanisms, the zinc oxide film is responsible for passivation. Using X-ray analysis, Powers[23] identified ZnO as the passive film; however, this analysis method, which requires the removal and subsequent drying

of the passive film, could have converted all the species to ZnO. In-situ identification data of the passivation film are not available. Two other hypotheses are that this film consists of either an underlying layer of $Zn(OH)_2$ with an overlay of ZnO[24-26] or a dual layer of ZnO, one formed by precipitation and the other by surface growth processes.[17,27] Powers and Breiter[17] considered the latter to be the cause of passivation. Recent results of optical and scanning electron microscopical observations[17,18,28,29] have indicated that the anodic formation of ZnO probably occurs via the precipitation-dissolution route. Szpak and Gabriel[18] illustrated that the sequential events of the dissolution-precipitation path for anodic ZnO formation are as follows: (a) establishment of a quasi-equilibrium adsorption region adjacent to the electrode; (b) development of a mass transport region next to the adsorption region; (c) formation of a polymerization region in which monomers are trapped; (d) transformation of the polymerization region into a nucleation and growth region; (e) formation of a zinc oxide film by merging of crystallites at the surface of the adsorption layer and subsequent growth of that film; and (f) collapse of oxide film due to mechanical factors resulting from the densification of the region adjacent to the adsorption region to reactivate zinc dissolution.

A number of investigators[7-14] have studied the correlation between current density and passivation time in the zinc electrode. A summary of these data reported in the literature is given in an Appendix. The current density, i, and passivation time, t, have been typically correlated by the equation,

$$(i - i_e)t^{1/2} = k \tag{2}$$

where i_e corresponds to diffusion-excluded convective current density, and k is a correlation constant. Equation 2 suggests that there is a current density, i_e, below which passivation will not occur. Assuming that during anodic dissolution the formation of a "critical" concentration of zincate at the electrode causes passivation and assuming that diffusion is the only mode of mass transport, Dirkse and Hampson[13] derived the equation:

$$i(t^{1/2}) = (C_{crit} - C_b)\ nF \left(\frac{\pi D}{4}\right)^{1/2} \tag{3}$$

where C_{crit} is the "critical" concentration of zincate for the precipitation of ZnO, C_b is the bulk concentration of zincate, n is the valency change of the electrode reaction, F is Faraday's constant, and D is the diffusion coefficient of zincate. Yamashita et al.[14] concluded from their chronoellipsometric study that two types of ZnO films form--type I film at time t_1 and type II film at t_2 --during galvanostatic oxidation. The correlation of current density and t_1 can be described by Eq. 3, while that of current density and t_2 can be represented by Eq. 2. Elder[12] interpreted the anodic characteristics of zinc in alkaline solution as a kinetically controlled process preceding a diffusion step, so that

$$i(t^{1/2}) = k_o - k_1 \cdot i \tag{4}$$

In summary, a review of the literature showed that zinc oxide is responsible for passivation of the zinc anode and that the presently accepted mechanism for the formation of this zinc oxide is a precipitation-dissolution model. The correlation between passivation time and current density has been typically expressed by Eq. 2. In our investigations, we conducted further experiments on the effects of current density (from 30 up to 1620 mA/cm^2) on passivation time of a small zinc anode with a KOH electrolyte (0.784 to 7.24M) in an experimental cell-testing apparatus. From these data, we estimated the effect of passivation time on the utilization of a zinc anode in an alkaline battery.

II. EXPERIMENTAL

Zinc electrodes were cut into dimensions of 0.05 by 0.13 cm from a zinc sheet of 99.99% purity purchased from United Mineral & Chemical Corp. (New York, NY). The impurities are as follows: Cd, 5 ppm; Pb, 5 ppm; Fe, 3 ppm; Cu, 2 ppm; Au, 1 ppm; Sn, 1 ppm; Ge, 0.5 ppm; and In, 0.5 ppm. The zinc electrodes were prepared for testing by polishing them with emery paper (No. 600). After preparation, they were horizontally mounted in an experimental apparatus (see Fig. 1) in either the facing-upward or -downward position.

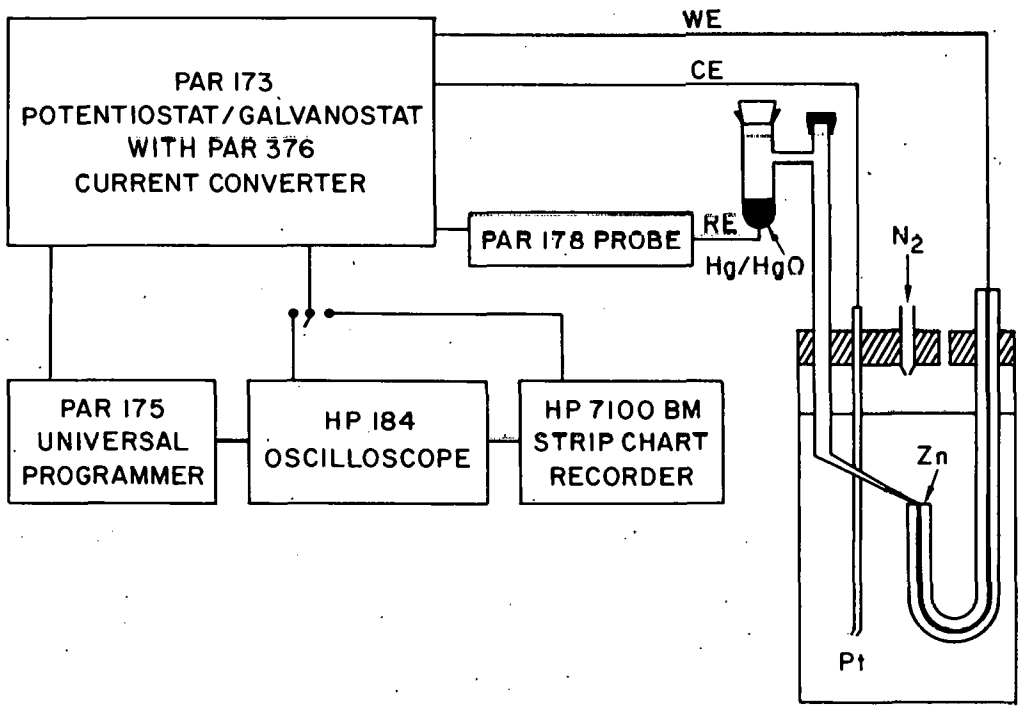

Fig. 1. Experimental Apparatus for Testing of Zinc Anodes in KOH Electrolyte (CE = counter electrode, WE = working electrode, and RE = reference electrode)

To eliminate edge effects, these zinc electrodes were set in acrylic plastic purchased from Fulton Products Corp. (Saxonberg, PA). The electrolyte was KOH at concentrations of 0.784, 2.92, 4.98, and 7.24M; in addition, 7.24M KOH saturated with zinc oxide was also used. The KOH was reagent grade, and the zinc oxide was analytical reagent quality. The above electrolyte solutions were prepared with doubly distilled water and deaerated by passing a stream of purified nitrogen through. The counter electrode was a 1-cm wide platinum strip. The anode potential was measured with an Hg/HgO reference electrode in conjunction with a Luggin capillary that had been placed as close to the anode surface as practical. A Model 173 Potentiostat/Galvanostat equipped with a Model 376 Current Converter (Princeton Applied Research Corp., Princeton, NJ) was used to provide constant current. The passivation time was determined to the instant that the anode potential was seen to increase rapidly. For a passivation time less than 6 s, a Model 184A Oscilloscope with a Model 1805A Dual Channel Vertical Amplifier and a Model 1825A Time Base and Delay Generator (Hewlett-Packard Co., Palo Alto, CA) was used to record the potential as a function of time; for a passivation time longer than 6 s, a Model 7100BM Strip Chart Recorder (Hewlett-Packard) was used. A Model 175 Universal Programmer (Princeton Applied Research) was programmed to trigger the potentiostat/galvanostat and the oscilloscope simultaneously.

The passivation times of the zinc electrodes polarized at a wide range of current densities were measured at room temperature (20°C). Before each measurement, the zinc electrode was anodically etched at 10μA for 5 s. After waiting for at least 10 min to ensure a quiescent state of the electrolyte and the establishment of electrode equilibrium state, polarization was commenced. Once passivated, electrodes were repolished. Potential/time oscilloscope traces were recorded photographically. Measurements were sometimes repeated to ensure reproducibility.

III. RESULTS

Table 1 lists the passivation time of facing-upward and -downward zinc microelectrodes discharged at current densities ranging from 61 to 1620 mA/cm^2 in 7.24M KOH electrolyte, as well as the passivation time of facing-upward electrodes discharged at 122 to 1530 mA/cm^2 in KOH saturated with ZnO. At some current densities, more than one passivation measurement was made to check the reproducibility of the test results. In addition, data were obtained using an electrode with about 1-mm deep plastic channel to reduce natural convection. The data in Table 1 are plotted in Fig. 2; the lines in this figure are a least-squares fit of the data. As can be seen in this figure, for passivation times less than 6 s, the facing-upward and facing-downward anodes have similar correlation between passivation times and current densities; however, for passivation times longer than 6 s, a facing-downward anode has a longer passivation time at a given current density. This figure also shows that the presence of zincate in the electrolyte shortens the passivation time.

Table 2 lists the passivation times of facing-upward anodes discharged at a wide range of current densities in three different concentrations of KOH (0.784, 2.92, and 4.98M); Fig. 3 shows these data in graph form as well

Table 1. Galvanostatic Polarization of Zinc Anodes in 7.24M KOH Electrolytes at Room Temperature (20°C)

No Zincate in Electrolyte				Electrolyte Saturated with ZnO	
Upward Electrode		Downward Electrode		Upward Electrode	
Current Density, mA/cm^2	Passivation Time, s	Current Density, mA/cm^2	Passivation Time, s	Current Density, mA/cm^2	Passivation Time, s
1530	0.50	1620	0.475	1530	0.340
1530	0.60	1620	0.380	1530	0.320
1370	0.76	1440	0.515	1220	0.500
1370	0.68	1440	0.535	1220	0.505
1220	1.01	1240	0.780	916	1.01
1220	0.91	1240	0.870	916	1.00
1220	0.76	1050	1.08	610	2.725
1070	1.14	1050	1.09	610	2.70
1070	1.28	858	1.875	305	15.64
916	1.51	668	3.50	305	15.44
916	1.78	525	7.08	153	439.2
763	2.51	477	11.48	122	1214.4
763	3.00	429	59.6		
763	3.34	382	156.2		
610	5.20	382	74.8		
610	4.12	382	54.6		
610	4.52	382	170.6		
458	8.20	334	161.2		
458	9.36	286	390.0		
305	22.9	191	2794.8		
305	32.4	141	8706.0		
223	184.8				
233	133.6	429	7.68[a]		
153	1970.4	382	61.3[a]		
122	2544.0	334	55.2[a]		
91.6	4432.8	286	3151.2[a]		
61.0	10848.0				

[a]A 1-mm deep channel has been created by chemical etching before the polarization was measured.

as the data from the facing-upward anode in 7.24M KOH from Fig. 2. As can be seen in this figure, a higher concentration of KOH will result in a longer passivation time for a zinc electrode at a given current density; therefore, a high concentration of KOH should result in increased zinc electrode lifetime.

Using the data from Tables 1 and 2, we determined the correlation constants of Eq. 2 (k, i_e) for zinc microelectrodes in the KOH electrolyte; the

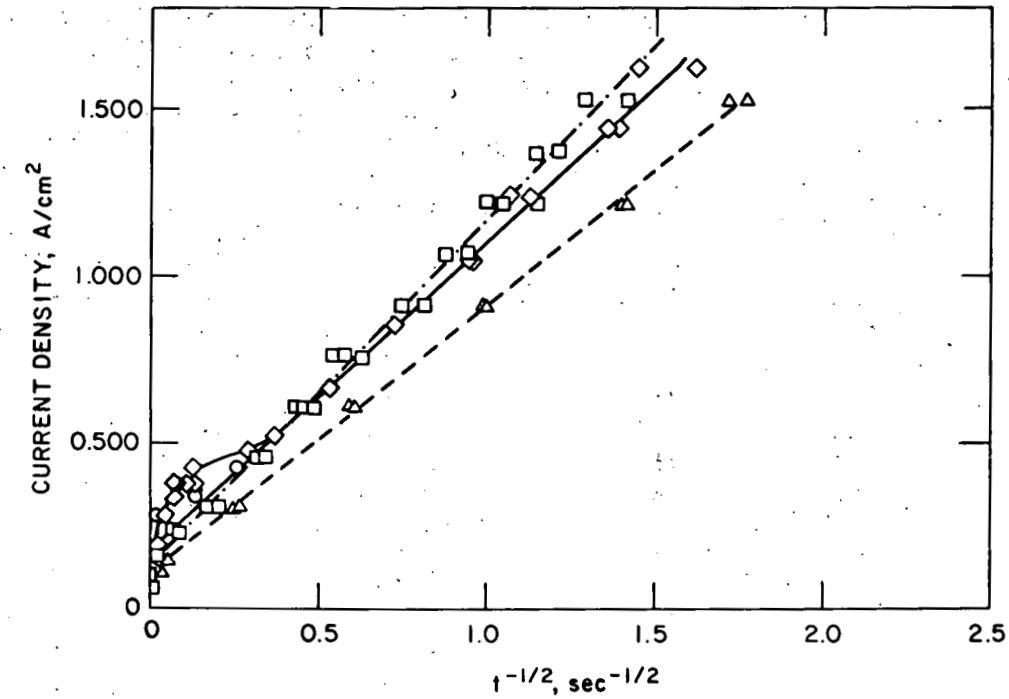

Fig. 2. Current Density vs. Passivation Time of the Zinc Anode in 7.24M KOH (squares, upward anode; diamonds, downward anode; circles, downward anode with 1-mm plastic channel; triangles, upward anode and saturated with zincate)

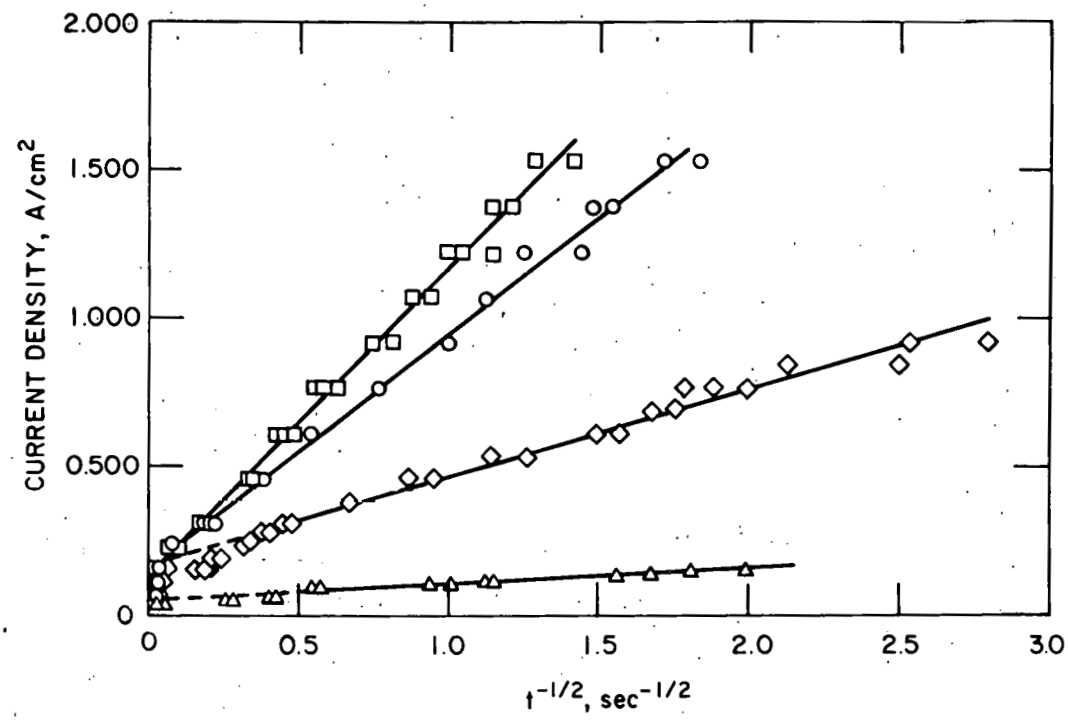

Fig. 3. Current Density vs. Passivation Time for Facing-Upward Anode in 7.24M (squares), 4.98M (circles), 2.92M (diamonds), and 0.784M (triangles) KOH Electrolyte.

Table 2. Galvanostatic Polarization of the Facing-Upward Zinc Anodes in Three Concentrations of KOH Electrolyte at Room Temperature (20°C)

4.98M KOH		2.92M KOH		0.784M KOH	
Current Density, mA/cm^2	Passivation Time, s	Current Density, mA/cm^2	Passivation Time, s	Current Density, mA/cm^2	Passivation Time, s
1530	0.30	916	0.128	153	0.305
1530	0.338	916	0.156	153	0.250
1370	0.46	839	0.160	137	0.410
1370	0.42	839	0.223	137	0.355
1220	0.48	763	0.315	122	0.760
1220	0.64	763	0.283	122	0.780
1070	0.78	763	0.253	107	0.980
1070	0.805	687	0.355	107	1.13
916	0.99	687	0.325	91.6	1.70
763	1.70	610	0.450	91.6	1.85
1610	3.4	610	0.405	76.3	3.25
458	7.06	534	0.665	76.3	3.03
458	8.30	534	0.770	61.0	5.40
305	24.4	458	1.110	61.0	5.50
229	176.0	458	1.320	45.0	14.02
153	979.2	382	2.225	45.0	12.95
122	1673.0	382	2.400	30.5	872.4
91.6	3705.6	305	4.40	30.5	1464.0
61.0	8448.0	305	4.75		
		275	6.10		
		275	5.85		
		244	8.66		
		244	9.68		
		229	22.28		
		191	16.12		
		191	29.0		
		153	44.2		
		153	29.4		
		153	29.2		
		122	745.2		
		122	689.2		
		91.6	2325.6		
		61.0	6240		

results are shown in Table 3. Table 1 shows that, for the facing-upward anode in 7.24M KOH, the passivation times were significantly longer at current densities $\leq$ 153 mA/cm^2. Therefore, in Table 3, correlation constants for this

Table 3. The Correlation Constants ($i = kt^{-1/2} + i_e$) of the Zinc Anodes

Electrode Orientation	Electrolyte, M	Current Density Range, mA/cm^2	Correlation Constants k, mA-s$^{1/2}$/cm^2	Correlation Constants i_e, mA/cm^2
Upward[a]	7.24	200-1530	1.03(± 0.02)x10^3	1.32(± 0.19)x10^2
		60-153	6.86(± 0.70)x10^3	-8.05(± 12.15)
Downward[a]	7.24	625-1620	9.23(± 0.49)x10^2	1.86(± 0.57)x10^2
Upward and Downward[a]	7.24	525-1620	9.48(± 0.30)x10^2	1.88(± 0.30)x10^2
Upward[a]	7.24 (Saturated with ZnO)	200-1530	8.06(± 0.11)x10^2	1.08(± 0.13)x10^2
		0-122	4.25 x 10^3	0
Upward[b]	4.98	200-1530	7.79(± 0.18)x10^2	1.69(± 0.20)x10^2
		60-153	4.26(± 0.22)x10^3	1.77(± 0.50)x10^1
Upward[b]	2.92	300-916	2.91(± 0.09)x10^2	1.76(± 0.14)x10^2
		60-122	2.32(± 0.29)x10^3	3.64(± 0.85)x10^1
Upward[b]	0.784	60-153	5.41(± 0.35)x10^1	5.18(± 0.44)x10^1

[a]Correlation constants determined from data in Table 2.

[b]Correlation constants determined from data in Table 3.

electrode-electrolyte system are given for two current density regions--above and below 153 mA/cm^2. For similar reasons, the correlation constants for facing-upward anodes in 7.24M KOH saturated with ZnO, 4.98M KOH, and 2.92M KOH are given in two separate current density regions. Since insufficient data were collected, correlations were given for only one current region in the cases of a facing-downward anode with 7.24M KOH electrolyte and a facing-upward anode with 0.784M KOH electrolyte. The correlation constant given for the low current region of the facing-upward anode with 7.24M KOH saturated with ZnO was calculated from the datum at 122 mA/cm^2, assuming zero intercept of the i vs. $t^{-1/2}$ curve.

IV. DISCUSSION AND CONCLUSIONS

A. One-Dimensional Diffusion Model

To justify the validity of Eq. 2, Dirkse and Hampson[13] proposed a one-dimensional diffusion model in which the accumulation of zincate ions at the electrode surface is the determining step of passivation. However, for an

electrode reaction controlled by a diffusional mass transport, the one-dimensional model is valid only if the following three factors are minimal: mass transfer by convection of zincate ion induced by the net changes of volume due to the electrochemical and chemical reactions,[30] migration, and three-dimensional diffusion. The following discussion shows that these three mass transport mechanisms can indeed be neglected for passivation times less than 14 s.

For the anodic reaction of the zinc electrode (see reaction 1), the net change of volume in the solid electrode and in the species in the electrolyte induces a superficial average velocity for the electrolyte, which is given by the equation,[31]

$$v^{\square} = \frac{-i}{nF}\left[\bar{V}_{Zn} + 4\bar{V}_B - \bar{V}_A - 2(t_2^{\circ}\bar{V}_A + t_3^{\circ}\bar{V}_B)\right] \tag{5}$$

where $\bar{V}_{Zn}$, $\bar{V}_A$, and $\bar{V}_B$ are the partial molar volumes of zinc, potassium zincate, and potassium hydroxide, respectively; and t_2° and t_3° are the transference numbers of zincate and hydroxide ions, respectively. A $v^{\square}$ of -1.5×10^{-4} cm/s was obtained by substituting into Eq. 5 data given by Sunu[31]--$\bar{V}_{Zn}$, 9.15 cm^3/mol; $\bar{V}_A$, 67.0 cm^3/mol; $\bar{V}_B$, 17.8 cm^3/mol; t_2°, 0.05; and t_3°, 0.72--and a current density of 1.53 A/cm^2. (The negative sign of the value for $v^{\square}$ means that the flow is in the direction opposite to the electrode surface.) When $v^{\square}$ is included, the one-dimensional mass transfer equation becomes

$$\frac{\partial C}{\partial t} + v^{\square}\frac{\partial C}{\partial x} = D\frac{\partial^2 C}{\partial x^2} \tag{6}$$

where C is the concentration of zincate ion, D is the diffusion coefficient of zincate ion, and x is the distance from the electrode surface. No analytical solution of Eq. 6 can be obtained for the present system. However, when $v^{\square}$ is considered as a perturbation of a one-dimensional diffusion, the solution to Eq. 6 can be approximated as

$$C_{crit} - C_b = \left(\frac{i}{F}\right)\left[\left(\frac{t}{D}\right)^{1/2} + \left(\frac{v^{\square}}{2D}\right)t\right] \tag{7}$$

Numerical calculations indicate that $v^{\square}$ could account for only 5% of the time controlled by a diffusion process. Thus, convection induced by the net change in volume of the solid electrode and electrolyte is minimal.

The possibility of three-dimensional diffusion must be considered since small electrodes were used to achieve uniform current density in our study. A three-dimensional diffusion in an isotropic medium takes the form of

$$\frac{\partial C}{\partial t} = D\left(\frac{\partial^2 C}{\partial r^2}\right) + \frac{2}{r}\left(\frac{\partial C}{\partial r}\right) \tag{8}$$

where r is the radial coordinate of a spherical geometry. With the proper initial and boundary conditions, one can show that the solution of Eq. (8) can be written as:

$$C_{crit} - C_b = \frac{i}{nF}\left(\frac{a}{D}\right)\left[1 - \exp\left(\frac{Dt}{a^2}\right) \text{erfc}\left(\frac{Dt}{a}\right)\right] \quad (9)$$

where the error function, erfc(x), is defined as

$$\text{erfc}(x) = 1 - \text{erf}(x) = \frac{2}{\sqrt{\pi}}\int_x^\infty e^{-x^2}\, dx \quad (10)$$

and a is the radius of a spherical electrode. For a small value of $(Dt)^{1/2}/a$ (e.g., 0.2), the bracket term in Eq. 9 can be approximated as $2(Dt/\pi)^{1/2}/a$; and therefore can be rearranged to Eq. 3. If the electrode surface can be approximated as a semisphere with a base area equal to the surface area of the electrode (6.5×10^{-3} cm^2), then a is calculated to be 4.5×10^{-2}cm. With this value of a, $D = 6 \times 10^{-6}$ cm^2/s,[32] and $(Dt)^{1/2}/a = 0.2$, we obtain a value of passivation time of 14 s below which the one-dimensional diffusion model is valid.

If mass transfer of zincate by migration is incorporated into the diffusion model, the current density, i, is multiplied by a factor of one plus t_2^o. Since the size of zincate ion is relatively large compared with the sizes of potassium and hydroxide ions, the transference number of zincate ion is expected to be small (Sunu[31] gave a value of 0.05). Therefore, the effect on passivation time of mass transfer of zincate ions by migration is minimal.

Since the effects of mass transfer of zincate ions by convection, migration, and three-dimensional diffusion are minimal for passivation times below 14 s, the value of i_e in Eq. 2 should be zero, and a combination of Eqs. 2 and 3 yields

$$k = (C_{crit} - C_b)\, nF\left(\frac{\pi D}{4}\right)^{1/2} \quad (11)$$

The calculated values of k using Eq. 11 are compared with the values obtained from our experimental data in Table 4. Although the calculated values of k are from 0.86 to 1.49 times the experimental values, the values of i_e given in Table 3 are not zero. This discovery will be discussed later; however, before we do so, we will compare our results with those of previous studies.

B. Comparison with Previous Studies

The linear increase of potential with time before the onset of passivation of our zinc microanodes is shown in Fig. 4a for a current density of 1.22 A/cm^2 and Fig. 4b for 0.61 A/cm^2. This effect was also observed by Dirkse and Hampson.[13] The overpotential increase may be mainly due to increases in the

Table 4. Comparison of the Experimental Values of Correlation Constants (k)

Electrode Orientation	Concentration of KOH, M	Diffusion Coefficient of Zincate Ion,[a] cm^2/s	"Critical" Concentration of Zincate ion,[b] M	Bulk Concentration of Zincate ion, M	Correlation Constant, $mA\text{-}s^{1/2}/cm^2$	
					Experimental	Eq. 11
Upward	7.24	6×10^{-6}	2.3	0	$1.03(\pm 0.02) \times 10^3$	9.64×10^2
Downward	7.24	6×10^{-6}	2.3	0	$9.23(\pm 0.49) \times 10^2$	9.64×10^2
Upward	7.24 sat'd with ZnO	6×10^{-6}	2.3	0.64	$8.06(\pm 0.11) \times 10^2$	6.95×10^2
Upward	4.98	8×10^{-6}	1.4	0	$7.79(\pm 0.18) \times 10^2$	6.77×10^2
Upward	2.92	1.0×10^{-5}	0.8	0	$2.91(\pm 0.09) \times 10^2$	4.33×10^2
Upward	0.784	1.2×10^{-5}	0.1	0	$5.41(\pm 0.35) \times 10^1$	3.93×10^1

[a]Data based upon information in Ref. 32.
[b]Data based upon information in Ref. 33.

ohmic resistance of the system. The short-life transition preceding the onset of passivation of zinc electrodes at the low current density (Fig. 4b) has also been observed by Bartelt and Landsberg[7] and Elder.[12] Since the electrode potential at the transition is in the vicinity of the Zn/ZnO standard potential, the transition may be associated with the direct formation of the passivating type II ZnO film observed by Powers et al.[17]

Although Hampson et al.[8,11,13] have claimed that no evidence could be found for any change in slope of the i vs. $t^{-1/2}$ curves as observed earlier by Landsberg and Bartelt,[5] our results (Figs. 2 and 3) indicate that there are upper and lower current density regions, each of which has a different correlation constant (see Table 3) for the facing-upward anodes. Hampson et al.[8,11,13] and Eisenberg et al.[6] reported that i_e in Eq. 2 is associated with natural convection. If this were true, extrapolation of the data obtained in the high current-density region would yield intercepts at zero, but the data in Figs. 2 and 3 contradict this assumption.

Yamashita et al.[14] measured the optical phase shift on a zinc electrode during a constant current discharge. They concluded that, at the first major phase shift, the electrolyte at the electrode surface becomes saturated with zincate and type I zinc oxide film begins to form and grow on the anode, and that, at the second major phase shift, the electrode becomes fully covered by compact type II zinc oxide film and thus passivated. Using ellipsometry and

(a)

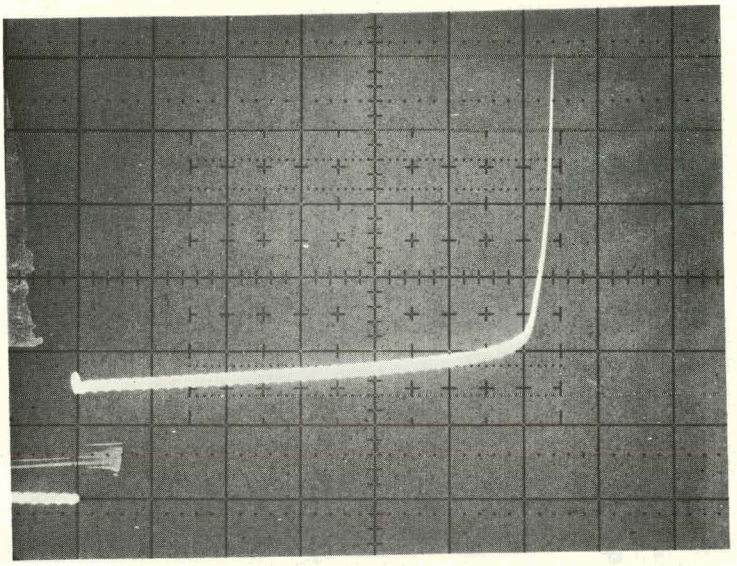

i = 1.22 A/cm^2 (Y-axis, 0.1 V/division;
X-axis, 0.1 s/division)

(b)

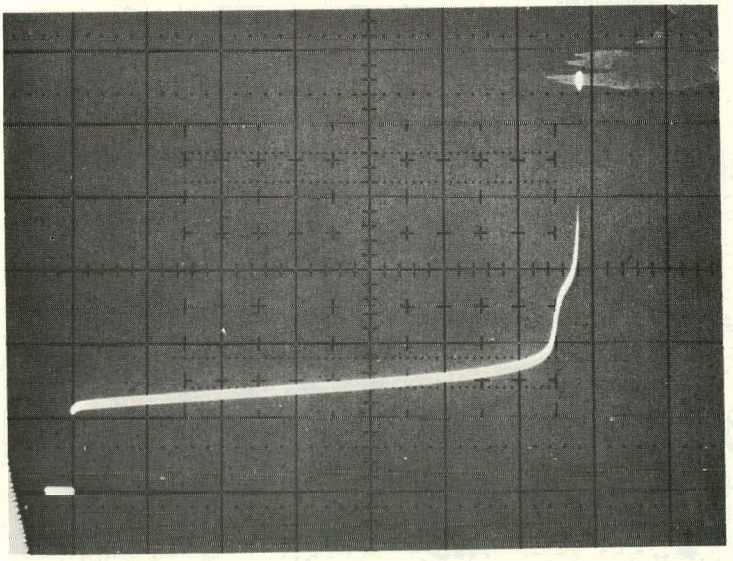

i = 0.61 A/cm^2 (Y-axis, 0.1 V/division;
X-axis, 0.5 s/division)

Fig. 4 Chronopotentiograms of Zinc Microanodes (4.98M KOH, Facing-Upward).

scanning electron microscopy, Smith has studied the anodic film growth of silver oxide, zinc oxide, and cadmium oxide under stagnant and forced convection conditions. He concluded that the process of anodic film growth of zinc oxide begins with roughening of the metal substrate and the growth of a mass transfer boundary layer, then the formation of "primary films," and finally passivation by a "compact primary layer" (porosity, about 0.003). This process is not in agreement with the hypothesis of Hampson et al.,[8,11,13] who have stated that passivation occurs when C_{crit} of zincate is established in the layer of electrolyte in contact with the electrode surface. We subsequently calculated the passivation times by substituting into Eq. 3 the diffusion coefficient data of zincate given by McBreen and Cairns[32] and the solubility limit of zincate (equal to half of bulk OH^- concentration as assessed by Hampson et al.[11,34]). This calculation resulted in passivation times that were only 1.5-8.4% of those given in Tables 1 and 2 for the low current density region. Therefore, the hypothesis of Hampson et al. does not explain our data.

It is generally postulated that passivation occurs when a "critical" concentration of zincate, usually three times chemical saturation, is established in the layer of electrolyte in contact with the electrode surface.[10,13] Since the density of a KOH electrolyte increases with increasing zincate content, natural convection can easily develop at the vicinity of the surface of a facing-downward electrode when the passivation time is less than one minute.[35] The facing-upward anode should effectively suppress this natural convection since the anode can hold zincate ions. Therefore, a divergence in the passivation times for the electrodes of these two orientations in 7.24M KOH occurs when the passivation time is longer than 6 s (see Fig. 2). The data in Table 1 for the facing-downward electrode with a plastic channel of 1-mm depth indicate that natural convection has been reduced to a certain extent, but not completely, by the shear stress exerted by the plastic channel wall.

V. PROPOSED ANODIC PROCESSES OF ZINC

In order to explain our experimental data, we propose the following scheme, shown in Fig. 5, for the processes associated with the anodic passivation of zinc in alkaline solutions. In the first step, the anodic reaction yields zincate, which accumulates near the electrode surface since diffusion is not fast enough to dissipate the newly formed zincate. In the next step, the accumulation of zincate results in a C_{crit} at which the rate of formation of type I film through a precipitation and dissolution mechanism becomes appreciable. The time at which C_{crit} is achieved, t_a, can be estimated by using Eq. 3, provided that D and C_{crit} are known. The value of C_{crit} is believed to be a factor of three to four times the solubility of ZnO in KOH solution and has an upper limit equal to half of the bulk OH^- concentration;[11,13,14,34,36,37] C_{crit} will be the same whether in a zinc oxide saturated solution or an electrolyte initially free from zincate.[37] In Eq. 3, the term $C_{crit} - C_b$ implies that the presence of zincate in the electrolyte shortens the passivation time; our results confirm this (see Table 1 and Fig. 2) conjecture. However, it is very difficult to detect on chronopotentiograms the time at which C_{crit} occurs, unless other means, such as an ellipsogram, are made available. The transformation of zincate to zinc oxide (type I) and mass transport of OH^- ions through

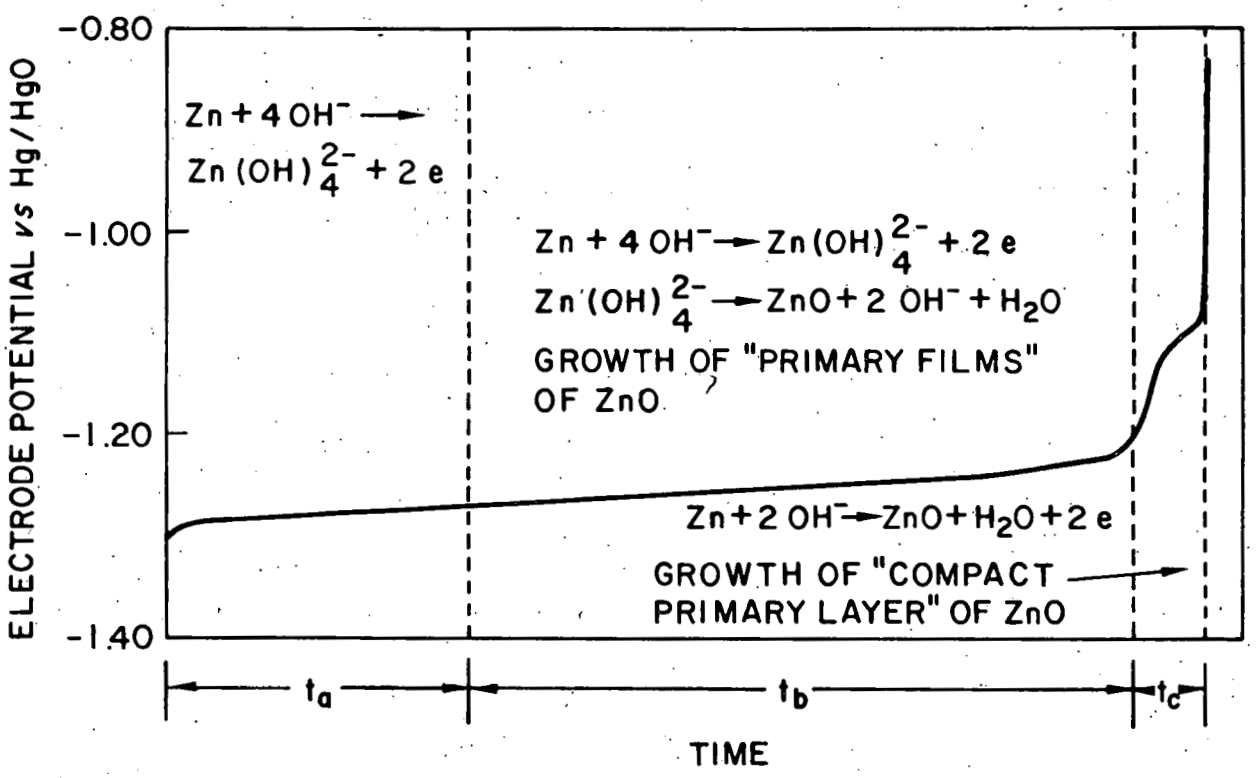

Fig. 5. Proposed Scheme for the Processes Associated with the Anodic Passivation of Zinc in Alkaline Solutions.

this porous zinc oxide[17] permit the continuation of the electrode reaction. After the passage of another period of time, t_b, the electrode potential reaches the vicinity of -1.20 volts vs. Hg/HgO, which is approximately the Zn/ZnO standard potential;[17,38] at this point, formation of zinc oxide (type II) is initiated on the electrode surface. In the final period of time, t_c, the electrode surface is totally covered by this compact type II ZnO, limiting the transport of OH^- ions. In this manner, the electrode becomes passivated. This proposed mechanism agrees with the observation of anodic film growth of zinc oxide by Smith using ellipsometry and a scanning electron microscope.[33]

According to the proposed mechanism, the passivation time can be expressed by the equation:

$$t = t_a + t_b + t_c \qquad (15)$$

where t_a is the time at which C_{crit} is established, and t_b and t_c are the times during which type I and type II ZnO films, respectively, are formed. Yamashita et al.[14] were the first to use the chronoellipsometry method to determine t_a, t_b, and t_c. Figure 6 shows t, t_a, and t_b plus t_c at different current densities for the zinc anodes (area, 2.1 cm^2) in 2.8M KOH tested by

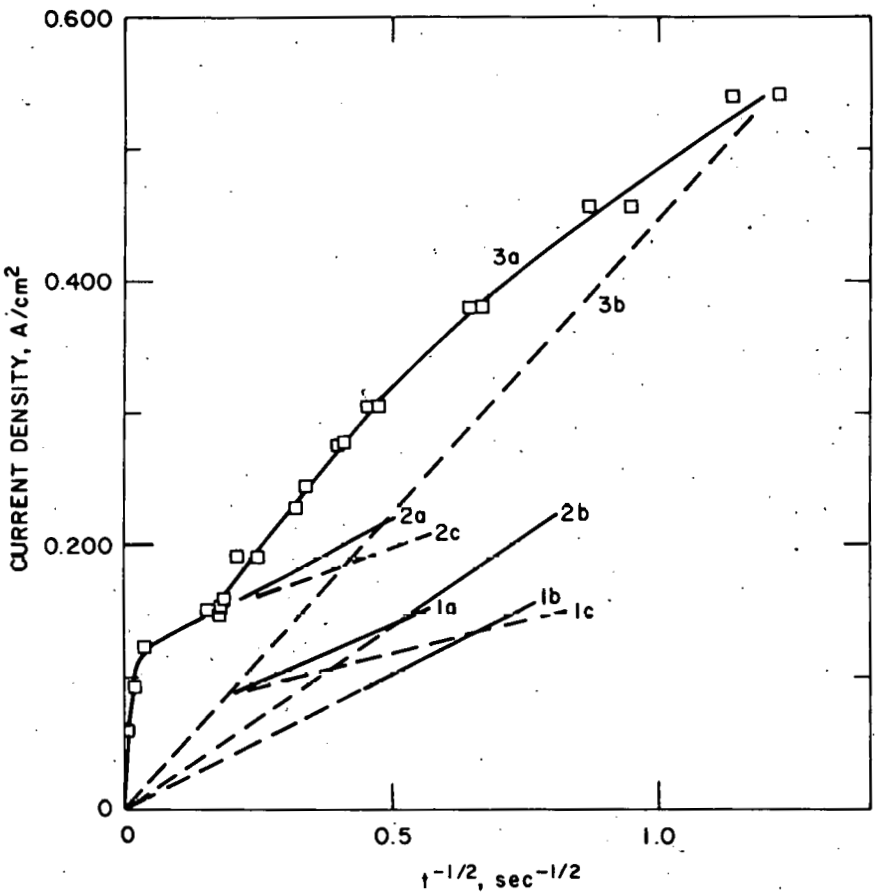

KOH Concentration, M	Diffusion (t_a)	Growth of Type I and II ZnO Films (t_b and t_c)	Overall Passivation Time (t)	Reference
2.0	1b	1c	1a	14
2.8	2b	2c	2a	14
2.92	3b	-	3a	this work

Fig. 6. Current Density vs. Passivation Times for Zinc Anodes (2.1 cm^2) in 2.0 and 2.8M KOH (Experiment Conducted by Yamashita et al.[14])

Yamashita et al. For this figure, t_a and t represent experimentally measured values; t_b plus t_c was then easily determined from Eq. 15. Also included in Fig. 6 are our passivation data for the zinc electrode in 2.92M KOH; the value of t_a for this electrode was generated by substituting the solubility data of electrochemically generated ZnO[36] and the diffusion coefficient of zincate[32] into Eq. 3. Figure 7 shows passivation-time data for one of our

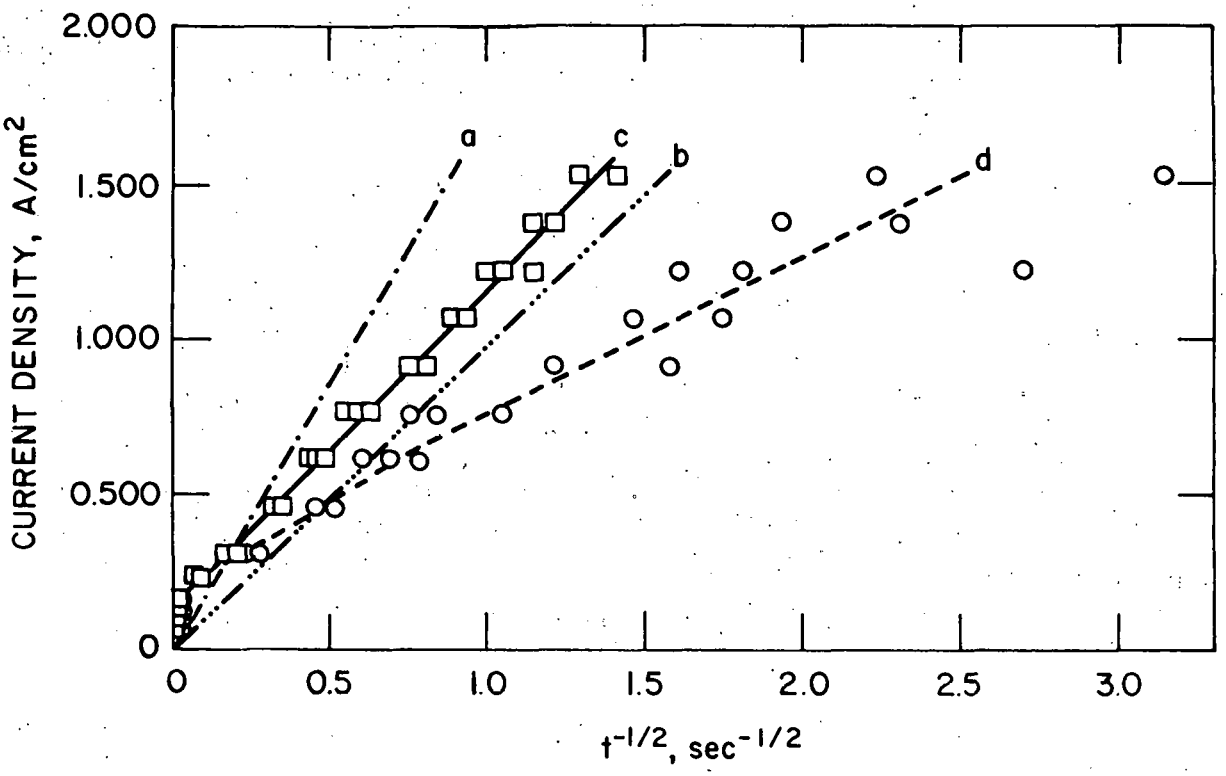

Fig. 7. Current Density vs. Passivation Time for Facing-Upward Zinc Anodes in 7.24M KOH (significance of the different lines is explained in the text).

facing-upward anodes in 7.24M KOH. Line (a) represents passivation time caused only by a simple exhaustion of OH^- species at the electrode surface and no precipitation; line (b) represents t_a and was determined in the same manner as used for Fig. 6; line (c) shows our passivation-time data; and line (d) was derived from lines (c) and (b), i.e., $t - t_a$.

In Figs. 2 and 3, we obtained nonzero intercepts for our data in the region of high current densities because t_a is not the major component of t throughout this region of current densities. However, as shown in Table 3, the values of i_e for the passivation data of the region of low current densities are nearly zero. To explain these results, we propose that the passivation time is almost entirely spent on the anodic film growth of type I ZnO. The electrode passivates because the anodic reaction rates are limited by the transport of OH^- ions through this zinc oxide film.[33] In our experiments, the zinc electrodes were set in acrylic plastic. The anodic reaction of zinc (reaction 1) erodes the solid zinc and leaves space surrounded by the plastic wall for the growth of the type I ZnO film. This type I ZnO film has pores of about 7500 Å on the average[29] and a porosity of 0.003 to 0.85[33] and, thus, presents a mass transfer resistance to the system. To obtain

a quantitative description of the effect of mass transfer resistance of the type I ZnO film, we assumed that, at the electrode surface, the rate of supply of OH^- ions is equal to the rate of consumption of OH^- ions by the electrode reaction. Therefore,

$$\frac{4i}{nF} = \frac{\varepsilon^{(1+t_e)} D_3}{\delta} (C_{3b} - C_{3s}) + \left(\frac{-it_3^\circ}{z_3 F}\right) + \left(\frac{2y}{nF}\right) i \qquad (16)$$

where the term in the left-hand side is the consumption rate of OH^- ions according to reaction 1; and the terms on the right-hand side represent the supply of OH^- ions by diffusion, migration, and precipitation of ZnO (see Fig. 5), respectively. In Eq. 16, ε is the porosity; t_e is the tortuosity factor of the ZnO film; D_3 is the diffusion coefficient of OH^- ions; C_{3b} and C_{3s} are the concentrations of OH^- ions in the bulk electrolyte and at the electrode surface, respectively; t_3° and z_3 are the transference number and the charge of OH^- ions, respectively; y is the ratio of the rate of precipitation of ZnO to that of electrochemical formation of zincate; and δ is the thickness of mass-transfer boundary layer (assumed to be equal to the thickness of the ZnO film). The rate of increase in the thickness of the ZnO film can be written as:

$$\frac{d\delta}{dt} = \frac{\bar{V}_{ZnO}}{(1-\varepsilon)} \frac{yi}{nF} \qquad (17)$$

where $\bar{V}_{ZnO}$ is the partial molar volume of ZnO. Since, in the low current density region, the time required to establish the C_{crit} concentration is negligible compared with the passivation time, we may set δ equal to zero at $t = 0$. Thereby, we obtain the expression:

$$\delta = \frac{\bar{V}_{ZnO}}{(1-\varepsilon)} \frac{yi}{nF} t \qquad (18)$$

Combining Eqs. 16 and 18, we obtain

$$\frac{\bar{V}_{ZnO}}{(1-\varepsilon)} \frac{y}{nF} \left[\frac{(4 - 2y)}{nF} + \frac{t_3^\circ}{z_3 F}\right] i^2 t = \varepsilon^{(1+t_e)} D_3 (C_{3b} - C_{3s}) \qquad (19)$$

At the time when C_{3s} is equal to zero, the electrode passivates. Thus, we obtain

$$i\, t^{1/2} = \left\{ \frac{\varepsilon^{(1+t_e)} D_3 C_{3b}}{\frac{\bar{V}_{ZnO}}{(1-\varepsilon)} \frac{y}{nF} \left[\frac{(4 - 2y)}{nF} + \frac{t_3^\circ}{z_3 F}\right]} \right\}^{1/2} \qquad (20)$$

The right side of Eq. 20 represents the correlation constant, k (see Eq. 2), for the low current density region in Table 3. We may use these data to calculate the porosity of the ZnO film. It is likely that the value of y is close

to unity since the rate of mass transport of zincate ions from the electrode surface through the ZnO film to the bulk electrolyte is small compared with the rate of electrochemical formation of zincate ions (reaction 1). Using $t_e = 0.5$, $y = 1$, $D_3 = 3 \times 10^{-5}$ cm^2/s (Ref. 31), $\bar{V}_{ZnO} = 14.51$ cm^3/mol, $t_3^s = 0.72$ (Ref. 36), $z_3 = -1$, and the values of k in Table 4, we calculated that the porosities of the ZnO films are 1.3 in 7.24M KOH, 0.08 in 7.24M KOH saturated with ZnO, 0.09 in 4.98M KOH, and 0.06 in 2.92M KOH. These porosities of the ZnO films are within those observed by Smith.[38] At the end of each measurement of passivation time, we also observed a dark film covering the electrode surface. Therefore, we concluded that, in the low current density region, the electrode reaction of zinc is accompanied by the growth of type I ZnO film, and that the electrode passivates when the oxide film becomes so thick that the rate of mass transfer of OH^- ions through the film is less than the rate of demand of OH^- ions for the electrode reaction.

VI. APPLICATION TO BATTERY TECHNOLOGY

Passivation of the zinc electrode in alkaline batteries should be avoided if a maximum utilization of the electrode is to be achieved. In the Ni/Zn alkaline batteries under development for vehicle propulsion, the electrolyte is typically 30% KOH (7M) saturated with ZnO; and the zinc electrode is formed by in-situ electrodeposition of zinc onto the grid. Using the data from our tests, we were able to estimate the effect of passivation on the utilization of the formed zinc electrode in an alkaline battery. However, it should be noted that our experimental cells had excess electrolyte in comparison with a typical Ni/Zn battery, which usually has a limited amount of electrolyte. Therefore, the projections given below should be used with caution. In addition, our results do not take into account the nonuniformity of current density distribution that occurs on a battery electrode surface.

For our calculations, we assumed that an electrodeposited-zinc porous electrode for a Ni/Zn battery cycled at a 2-h rate has a current density of 20 mA/cm^2. Our results given in Table 3 are for planar electrodes. In order to apply these results to a porous electrode, we first assessed the effective interfacial surface area per square centimeter of macroscopic area and then calculated the corresponding current density in a porous electrode.

A knowledge of the structure of zinc electrodeposits is necessary to assess the effective interfacial surface area. Naybour[39] observed that the deposits were dendritic at 100 mA/cm^2, consisted of layer growths with some granular growths at 20 mA/cm^2, and were mossy or sponge growths at 4 mA/cm^2. The zinc electrode in a typical Ni/Zn battery consists of metallic sponge zinc.[40] A zinc porous electrode cycled at a 2-h rate (20 mA/cm^2) has a charge density of 144 C/cm^2. From the data of charge density as well as the size and density of sponge deposits given by Naybour,[39] we estimated the porosity of the deposits to be about 0.6. Using these data and the molar volume of solid zinc[31] (9.15 cm^3/mol), we calculated that the electrode has an average thickness of zinc deposits of 114 μm. This value of electrode thickness is slightly less than the characteristic reaction penetration depth, 90 μm.[41] Using this characteristic reaction depth rather than the electrode thickness and a specific

surface area of 300 cm^2/cm^3,[31] we obtained an effective interfacial surface area of 2.7 per square centimeter of electrode area. This effective interfacial surface area yields a current density of 7.4 mA/cm^2 in a planar electrode, which corresponds to 20 mA/cm^2 at the 2-h rate for a porous zinc electrode. Since the electrolyte is usually 30% KOH saturated with ZnO, the correlation equation in the range of operating current density for the electrolytes in Table 3 is

$$i = (4.25 \times 10^3 \text{ mA-s}^{1/2}/\text{cm}^2)\ t^{-1/2} \qquad (21)$$

where i is in mA/cm^2, and t is in s. When the current density of 7.4 mA/cm^2 is substituted into Eq. 21, we obtain a passivation time of 9.16 h, which is much longer than the rated period of 2 h. Assuming that the effective interfacial surface area remains constant, we estimated the maximum current density for a 100% utilization of the electrode without encountering passivation from Eq. 21 and the equation of utilization,

$$Q = 10^{-3}\ i \cdot t \qquad (22)$$

where Q is the capacity of the zinc electrode (C/cm^2) at passivation time, t, and the factor of 10^{-3} is used to convert the current density from mA/cm^2 to A/cm^2. For 100% electrode utilization, Q is equal to 144 C/cm^2. Therefore, we obtain a maximum current density of 125 mA/cm^2 in planar electrodes, which corresponds to a current density of 338 mA/cm^2 in the porous zinc electrode. A current density of 338 mA/cm^2 is 17 times the designed current density, and probably does not occur even under severe driving conditions. Therefore, we conclude that passivation would not limit the utilization of a newly formed zinc porous electrode.

ACKNOWLEDGMENT

We thank Z. Nagy for his valuable comments.

APPENDIX

Summary of Galvanostatic Data of Zinc in KOH Electrolytes From Previous Studies

Summary of Galvanostatic Data of Zinc in KOH Electrolytes From Previous Studies

Electrode	Temp., °C	Electrode Orientation	KOH Electrolyte Concent.	Current Density Range, mA/cm^2	Correlation Constants k, $mA\text{-}s^{1/2}/cm^2$	Correlation Constants i_e, mA/cm^2	Ref. No.
Zn encased in epoxy resin (surface area 0.1-0.2 cm^2)	20	not specified (horizontally facing downward is likely)	0.5M	15-25	-	7	7
			1.0M	40-80	-	20	
			1.5M	80-150	160	40	
			2.0M	120-220	180	70	
			2.5M	160-250	285	80	
			3.0M	200-300	340	90	
			3.5M	220-370	410	110	
			4.0M	230-400	450	140	
			5.0M	350-420	570	145	
			6.0M	400-530	680	140	
			2.0M	320-760	-	40	
			3.0M	540-1050	-	175	
			4.0M	760-1200	-	310	
			5.0M	950-1390	-	420	
Zn rectangular plate (surface area, 28.5 & 34.2 cm^2)		Horizontally facing upward and downward; Vertical	6.9M (sat'd with ZnO)	250-640	846	63.6	
Zn disk	25	Horizontally facing upward	1.0M	12-38	117.8	0.52	8
			2.0M	12-101	377.3	0.21	
			3.5M	24-221	766	1.49	
			5.0M	34-252	993	0.19	
			6.5M	49-201	1259	0.12	
			8.0M	302	1323	0.60	
			9.0M	302	1324	-0.79	
			10.0M	302	1311	-0.08	
			12.0M	352	1255	-0.92	
			13.8M	302	1015	-0.21	

(cont'd)

Summary of Galvanostatic Data of Zinc in KOH Electrolytes From Previous Studies (Cont'd)

Electrode	Temp., °C	Electrode Orientation	KOH Electrolyte Concent.	Current Density Range, mA/cm^2	Correlation Constants k, mA-s$^{1/2}$/cm^2	Correlation Constants i_e, mA/cm^2	Ref. No.
Zn disk	20	Vertical	1.0M	12-40	57	8.8	9
			2.0M	50-128	220	49	
			3.5M	88-222	420	74	
			5.0M	100-260	760	84	
Zn encased in teflon tube (surface area, 0.020 cm^2)	room temp.	Horizontally facing upward	6.9M			70	10
			6.9M (sat'd with ZnO)	-	-	62	
Zn(Hg)			6.9M			74	
			6.9M sat'd with ZnO)	-	-	93	
Zinc	23	Horizontally facing downward	7M	60-320	1330	0.0	11
			7M + 0.23M Zn (II)	60-320	1300	0.0	
			7M + 0.31M Zn (II)	60-320	1310	1.1	
			7M + 0.63M Zn (II)	60-320	1135	1.5	
			7M + 0.93M Zn (II)	60-320	1032	1.9	
			7M + 1.12M Zn (II)	60-320	1015	5.0	
					1030	5.	
			13M + 1.07 Zn (II)		810	13	
	50		13M + 2.42 Zn (II)		700	19	
			7M,		2110	0	
			7M + 0.45M Zn (II)		1900	5	
			7M + 0.89M Zn (II)		1350	7	

(cont'd)

Summary of Galvanostatic Data of Zinc in KOH Electrolytes From Previous Studies (Cont'd)

Electrode	Temp., °C	Electrode Orientation	KOH Electrolyte Concent.	Current Density Range, mA/cm^2	Correlation Constants k, mA-s$^{1/2}$/cm^2	Correlation Constants i_e, mA/cm^2	Ref. No.
Zn disk	25	Horizontally facing upward	6.9M	148-555	k_o = 1825[a] k_1 = 1121[a]		12
			6.9M saturated with ZnO	102-740	k_o = 907[a] k_1 = 696[a]		
Zn encased in polyethylene (surface area, 0.02 cm^2)	23	Horizontally facing downward	1M	2300-5000	122	0	13
			2M	2500-10000	310	0	
			3.5M	2500-10000	470	0	
			4.5M	2500-10000	770	0	
			5M	3000-10000	885	0	
			7M	4000-10000	1370	0	
			12.8M	5000-10000	1000	0	
	0		2M		112	0	
	40		2M		620	0	
	50		2M		890	0	
Zn sheet covered with resin (surface area, 2.1 cm^2)	24	Vertical	0.8M				
			0.8M sat'd with ZnO	-	48.1 ± 2.5	0	
			1.2M	-	102 ± 18.7	0	
			1.6M	-	140.8 ± 7.9	0	
			2.0M	-	200 ± 12	0	
			2.8M	-	277.8 ± 13.9	0	

[a] The data were correlated with the equation, $i \cdot t^{1/2} = k_o - k_1 \cdot i$.

(cont'd)

Summary of Galvanostatic Data of Zinc in KOH Electrolytes From Previous Studies (Cont'd)

Electrode	Temp., °C	Electrode Orientation	KOH Electrolyte Concent.	Current Density Range, mA/cm^2	Correlation Constants k, $mA\text{-}s^{1/2}/cm^2$	Correlation Constants i_e, mA/cm^2	Ref. No.
			0.8M	-	55.5 ± 2.6	14.06 ± 0.20	
			0.8M sat'd with ZnO	-	54.6 ± 0.6	7.65 ± 0.33	
			1.2M	-	119 ± 15.6	18.60 ± 2.33	
			1.6M	-	137 ± 3.8	35.00 ± 1.96	
			2.0M	-	172.4 ± 3.0	54.21 ± 2.55	
			2.8M	-	222.2 ± 4.9	109.6 ± 6.3	

REFERENCES

1. W. Van Doorne and T. P. Dirkse, J. Electrochem. Soc. 122, 1 (1975).
2. G. H. Newman and G. E. Blomgren, J. Chem. Phys. 43, 2744 (1965).
3. J. S. Fordyce and R. L. Baum, J. Chem. Phys. 43, 843 (1965).
4. R. Landsberg, Z. Phys. Chem. 206, 291 (1957).
5. R. Landsberg and H. Bartelt, Z. Elektrochem. 61, 162 (1957).
6. M. Eisenberg, H. F. Bauman, and D. M. Brettner, J. Electrochem. Soc. 108, 909 (1961).
7. H. Bartelt and R. Landsberg, Z. Phys. Chem. 222, 217 (1963).
8. N. A. Hampson and M. J. Tarbox, J. Electrochem. Soc. 110, 95 (1963).
9. N. A. Hampson, M. J. Tarbox, L. T. Lilley, and J. P. G. Farr, Electrochem. Technol. 2, 309 (1964).
10. T. P. Dirkse, D. DeWit, and R. Shoemaker, J. Electrochem. Soc. 115, 442 (1968).
11. N. A. Hampson, P. E. Shaw, and R. Taylor, Br. Corros. J. 4, 207 (1969).
12. J. P. Elder, J. Electrochem. Soc. 116, 757 (1969).
13. T. P. Dirkse, and N. A. Hampson, Electrochim. Acta 16, 2049 (1971).
14. M. Yamashita, T. Yoshimura, Y. Imanaka, and H. Furuta, Doshisha Daigaku Rikogaku Kenkyu Hokoku 18, 58 (1977).
15. R. N. Elsdale, N. A. Hampson, P. C. Jones, and A. N. Strachan, J. Appl. Electrochem. 1, 213 (1971).
16. G. Coates, N. A. Hampson, A. Marshall, and D. F. Porter, J. Appl. Electrochem. 4, 75 (1974).
17. R. W. Powers and M. W. Breiter, J. Electrochem. Soc. 116, 719 (1969).
18. S. Szpak and C. J. Gabriel, J. Electrochem. Soc. 126, 1914 (1979).
19. E. A. Ivanov, T. I. Popova, and B. N. Kabanov, Sov. Electrochem. 5, 643 (1969).
20. M. N. Hull and J. E. Toni, Trans. Faraday Soc. 67, 1128 (1971).

21. R. D. Armstrong, G. M. Bulman and H. R. Thirsk, J. Electroanal. Chem. 22, 55 (1969).

22. H. Kaesche, Electrochim. Acta 9, 383 (1964).

23. R. W. Powers, J. Electrochem. Soc. 116, 1652 (1969).

24. K. Huber, Helv. Chim. Acta 26, 1037 (1943).

25. K. Huber, J. Electrochem. Soc. 100, 376 (1953).

26. K. Huber, J. Electrochem. Soc. 48, 26 (1942).

27. R. W. Powers, J. Electrochem. Soc. 118, 687 (1971).

28. Z. Nagy and J. O'M Bockris, J. Electrochem. Soc. 119, 285 (1972).

29. T. Katan, J. R. Savory and J. Perkins, J. Electrochem. Soc. 126, 1835 (1979).

30. J. Newman and W. Tiedemann, AIChe J. 21, 25 (1975).

31. W. G. Sunu, Transient and Failure Analysis of Porous Zinc Electrodes, Ph. D. Thesis, Univ. of Calif., Los Angeles (1978).

32. J. McBreen and E. J. Cairns, Advances in Electrochemistry and Chemical Engineering 10, 273 (1978).

33. C. G. Smith, Ellipsometry of Anodic Film Growth, LBL-8082 (1978).

34. A. Marshall and N. A. Hampson, J. Appl. Electrochem. 7, 271 (1977).

35. P. Delahay, New Instrumental Methods in Electrochemistry, Interscience Publishers, Inc., New York, NY (1965).

36. A. G. Briggs, N. A. Hampson, and A. Marshall, Trans. Faraday Soc. 70, 1978 (1974).

37. A. Langer and E. A. Pantier, J. Electrochem. Soc. 115, 990 (1968).

38. H. H. Bode, V. A. Oliapuram, D. Berndt, and P. Ness, Zinc-Silver Oxide Batteries, A. Fleischer and J. L. Lander, Eds. John Wiley & Sons, Inc., New York, NY, p. 7 (1971).

39. R. D. Naybour, Electrochim. Acta 13, 763 (1968).

40. M. Klein and D. Dube, ANL-K76-3541-1 (1976).

41. M. B. Liu, Y. Yamazaki, G. M. Cook, and N. P. Yao, to be published.

Distribution for ANL/OEPM-80-1

Internal:

J. J. Barghusen
D. Barney
C. Bean
E. C. Berrill
M. Blander
A. Brown
L. Burris
F. A. Cafasso
G. Chapman
A. A. Chilenskas
E. Creamer
C. C. Christianson
G. Cook
D. Corp
W. DeLuca
R. C. Elliott
P. R. Fields
D. Fredrickson
B. R. T. Frost
G. T. Garvey
E. C. Gay
J. Geller
M. Genge
J. Harmon
F. Hornstra
C. C. Hsu
J. Klinger
V. Kremesec
A. B. Krisciunas
M. Krumpelt
M. Kronenberg
M. L. Kyle
W. W. Lark
T. Lee
M. Liu
R. Loutfy
W. E. Massey
C. A. Melendres
J. Miller
W. Miller
N. Minh
J. Meisenhelder
Z. Nagy
P. A. Nelson
D. Poa
J. Rajan
J. J. Roberts
M. F. Roche
H. Shimotake
R. K. Steunenberg
C. A. Swoboda
Z. Tomczuk
R. Varma
P. D. Vashishta
D. R. Vissers
D. S. Webster
N. P. Yao (60)
ANL Contract File
ANL Libraries (5)
TIS Files (6)

External:

DOE-TIC, for distribution per UC-94ca (315)
Manager, Chicago Operations and Regional Office, DOE
Chief, Office of Patent Counsel, DOE-CORO
V. Hummel, DOE-CORO
J. Purcell, Chicago Operations Office, Argonne, IL
President, Argonne Universities Association
Chemical Engineering Division Review Committee:
- C. B. Alcock, U. Toronto
- R. C. Axtmann, Princeton University
- J. T. Banchero, Univ. of Notre Dame
- T. Cole, Ford Motor Corp.
- P. W. Gilles, Univ. of Kansas
- R. I. Newman, Warren, N.J.
- H. Perry, Resources for the Future, Washington
- G. M. Rosenblatt, Pennsylvania State University
- W. L. Worrell, U. of Pennsylvania

S. Abens, Energy Research Corporation, Danbury, CT
E. T. Ames, TRW Systems, Redondo Beach, CA
S. J. Angelovich, Mallory Battery Co., Tarrytown, NY
G. M. Arcand, Idaho State University, Pocatello, ID
G. N. Ault, NASA-Lewis Research Center, Cleveland, OH
A. D. Babinsky, T.R. Evans Research Center, Painesville, OH
K. F. Barber, DOE, Office of Transportation Programs, Washington, DC
T. Barber, Jet Propulsion Laboratory, Pasadena, CA
T. M. Barlow, Lawrence Livermore Laboratory, Livermore, CA
D. Barron, Delco-Remy Div. GMC, Anderson, IN
R. G. Bautista, Iowa State U.
R. Bassett, Sandia Labs, Albuquerque, NM

L. Belove, Marathon Battery Corp., Waco, TX
D. N. Bennion, Brigham Young University, Provo, UT
J. B. Berkowitz, Arthur D. Little, Cambridge, MA
L. Berkowitz, Esso Research & Engineering Co., Linden, NJ
C. Berlsterling, Franklin Institute, Philadelphia, PA
E. Berman, TRW Systems Group., McLean, VA
K. Blurton, Institute of Gas Technology, Chicago, IL
D. P. Boden, C&D Batteries, Plymouth Meeting, PA
J. Bolger, University of California, Berkeley, CA
D. Bowman, United States Postal Service, Washington, DC
J. Brennand, General Research Corp., Santa Barbara, CA
P. Bro, J. R. Mallory & Co., Inc., Burlington, MA
E. P. Broglio, Eagle-Picher Industries, Joplin, MO
P. J. Brown, DOE, Office of Transportation Programs, Washington, DC
R. Buchholz, Honeywell Corp., Minneapolis, MN
T. Burgess, Lucas Industries, Troy, MI
H. Burghart, Cleveland State University, Cleveland, OH
B. W. Burrows, Gould Inc., Rolling Meadows, IL
E. Buzzelli, Westinghouse Electric Corp., Pittsburgh, PA
E. J. Cairns, Lawrence Berkeley Laboratory, Berkeley, CA
P. Campbell, University of Southern California, Los Angeles, CA
R. T. Carpenter, Kimberly Clark Corp. Neenah, WI
T. V. Carvey, Hughes Aircraft Corp., Culver City, CA
T. W. Chapman, U. of Wisconsin, Madison, WI
R. Childs, Energy Research & Development Corp., Olmsted Falls, OH
L. D. Christian, General Electric, Gainesville, FL
J. E. Clifford, Battelle Memorial Institute, Columbus, OH
P. D. Cole, Naval Ordnance Laboratory, Silver Spring, MD
J. G. Colin, Englehard Industries Inc., Edison, NJ
W. B. Collins, Martin Marietta Corp., Denver, CO
J. E. Cooper, Aero Propulsion Laboratory, Wright-Patterson AFB, OH
K. E. Cox, University of New Mexico, Albuquerque, NM
D. Davis, Lawrence Livermore Laboratory, Livermore, CA
P. Davis, DOE, Office of Transportation Programs, Washington, DC
R. J. Dawson, ESB Inc., Madison, WI
N. A. Demerdash, Virginia Polytechnic Institute, Blacksburg, VA
D. Dharia, Energy Research Corp., Danbury, CT
G. A. DiBari, International Nickel Co., New York, NY
W. J. Dippold, DOE, Office of Transportation Programs, Washington, DC
T. P. Dirske, Calvin College, Grand Rapids, MI
F. M. Donahue, U. of Michigan, Ann Arbor, MI
D. B. Eisenhaure, Charles Stark Draper Lab Inc., Cambridge, MA
M. W. Ellison, Hughes Aircraft Corp., El Segundo, CA
R. P. Epple, Div. of Material Sciences, U.S. DOE, Washington, DC
J. Evans, U. of California, Berkeley, CA
R. E. Evans, Johns Hopkins University, Silver Spring, MD
A. Ewing, DOE, Office of Transportation Programs, Washington, DC
F. Fedor, Bell Laboratories, Murray Hill, NJ
R. Ferraro, Electric Power Research Institute, Palo Alto, CA
A. Fleischer, Orange, NJ
R. F. Fogle, North American Rockwell, Anaheim, CA
R. T. Foley, American University, Washington, DC
J. S. Fordyce, NASA-Lewis Research Center, Cleveland, OH
G. S. Foerster, NL Metals/NL Industries, Hightstown, NJ

D. N. Goens, Hazen Research, Golden, CO
G. Goodman, Globe-Union Inc., Milwaukee, WI
R. E. Goodson, Purdue University, W. Lafayette, IN
C. B. Graff, NASA-George C. Marshall Space Flight Center, Huntsville, AL
J. A. S. Green, Martin Marietta Laboratories, Baltimore, MD
R. Guess, General Electric Research Lab, Schenectady, NY
R. G. Gunther, General Motors Research Labs, Warren, MI
G. Hagey, DOE, Division of Technology Overview, Washington, DC
G. Halpert, NASA-Goddard Space Flight Center, Greenbelt, MD
H. Hamilton, University of Pittsburgh, Pittsburgh, PA
B. Hamling, Zircar, Florida, NY
V. Hampel, Lawrence Livermore Laboratory, Livermore, CA
K. L. Hanson, General Electric Co., Philadelphia, PA
J. H. Harrison, Naval Ship R&D Center, Annapolis, MD
G. Hartman, ESB Incorporated, Yardley, PA
J. Hartman, General Motors Research Labs, Warren, MI
E. A. Henry, U. of California, Livermore, CA
V. Hlavin, NASA-Lewis Research Center, Cleveland, OH
G. Hobbib, ESB Inc., Cleveland, OH
J. E. Hoffmann, Exxon Research and Engineering Co., Florham Park, NJ
R. Hudson, Eagle-Picher Industries, Joplin, MO
H. L. Hughes, Oklahoma State University, Stillwater, OK
W. B. Iaconelli, Ionics Inc., Watertown, MA
G. H. Jantz, Rensselaer Polytechnic Institute, Troy, NY
W. P. Jensen, Idaho National Engineering Laboratory, Idaho Falls, ID
L. Jokl, MERADCOM, Fort Belvoir, VA
W. J. Jones, Westinghouse Electric Corp., Pittsburgh, PA
J. Jorné, Wayne State U., Detroit, MI
W. Juda, Prototech, Inc. Newton Highlands, MA
E. Kanter, Gulton Battery Corp., Metuchen, NJ
N. Kaplan, Harry Diamond Laboratories, Washington, DC
T. Katan, Lockheed Palo Alto Research Laboratory, Palo Alto, CA
J. A. Kerrella, Delco-Remy Division/GMC, Anderson, IN
R. A. Keyes, Robert A. Keyes Associates, Martinsville, IN
W. C. Kincaide, Teledyne Energy Systems, Timonium, MD
R. Kirby, U. S. Bureau of Mines, Washington, DC
R. S. Kirk, DOE, Office of Transportation Programs, Washington, DC
K. Klein, U. S. Department of Energy, Washington, DC
J. G. Krisilas, Aerospace Corporation, El Segundo, CA
V. Kudryk, ASARCO Inc., South Plainfield, NJ
A. Landgrebe, U. S. Department of Energy, Washington, DC
R. Lund, St. Joe Minerals Corp., Monaca, PA
J. Mader, Electric Power Research Institute, Palo Alto, CA
J. Maisel, Cleveland State University, Cleveland, OH
R. E. Maizell, Olin Research Center, New Haven, CT
V. Manson, National Aeronautics and Space Adm., Washington, DC
C. E. May, NASA-Lewis Research Center, Cleveland, OH
J. McBreen, Brookhaven National Laboratory, Upton, NY
B. McCormick, Los Alamos Scientific Labs, Los Alamos, NM
L. A. McCoy, E. I. duPont de Nemours & Co., Wilmington, DE
L. R. McCoy, Atomics International, Canoga Park, CA
J. McKeown, DOE, Office of Program Administration, Washington, DC
R. P. Mikkelson, General Dynamics, San Diego, CA
D. G. Miley, U. S. Naval Ammunition Depot, Crane, IN

F. J. Mollura, Rome Air Development Center, Griffiss AFB, NY
F. Moore, DOE, Energy Storage Systems, Washington, DC
J. Moseley, Dow Chemical R&D, Pittsburgh, CA
A. Moss, Leesona Moos Laboratories, Warwick, RI
T. Mukherjee, National Science Foundation, Washington, DC
J. P. Mulling, National Aeronautics and Space Adm., Washington, DC
G. Murphy, Northwestern University, Evanston, IL
N. T. Musial, NASA-Lewis Research Center, Cleveland, OH
H. V. Nadham, Bogue Batteries, El Segundo, CA
W. J. Nagle, NASA-Lewis Research Center, Cleveland, OH
M. M. Nickolson, Atomics International Division, Canoga Park, CA
K. Nobe, U. of California, Los Angeles, CA
J. Norberg, ESB Inc., Philadelphia, PA
W. Opie, AMAX Inc., Carteret, NJ
B. N. Otzinger, North American Aviation, Downey, CA
J. E. Oxley, Gould Inc., Rolling Meadows, IL
J. S. Parkinson, Johns-Manville R&D Center, Manville, NJ
C. Pax, DOE, Office of Transportation Programs, Washington, DC
J. P Pemsler, Castle Technology Corporation, Lexington, MA
G. F. Pezdirtz, DOE, Energy Storage Systems, Washington, DC
A. G. Plunckett, General Electric R&D Center, Schenectady, NY
V. J. Puglisi, Yardney Electric Corp., Pawcatuck, CT
E. Raskin, USAF Cambridge Research Laboratory, Bedford, MA
A. D. Raynard, AiResearch Manufacturing Co., Torrance, CA
H. L. Recht, Atomics International Division, Canoga Park, CA
E. Rizkalla, DOE, Washington, DC
L. Rosenblum, NASA-Lewis Research Center, Cleveland, OH
N. Rosenburg, Department of Transportation, Cambridge, MA
R. Rosey, Westinghouse Electric Corp., Pittsburgh, PA
J. W. Ross, Texas Instruments Inc., Attleboro, MA
J. Rossmon, Cornell University, Ithaca, NY
G. Rowland, General Electric, Schenectady, NY
J. Rubenzer, NASA-Ames Research Center, Moffett Field, CA
A. J. Salkind, Rutgers Medical School
I. O. Salyer, Monsanto Research Corp., Dayton, OH
F. J. Salzano, Brookhaven National Laboratory, Upton, NY
D. F. Schmidt, General Electric Co., Washington, DC
L. W. Schopen, NASA-Lewis Research Center, Cleveland, OH
S. Schuldiner, Naval Research Laboratory, Washington, DC
W. R. Scott, TRW Systems Inc., Redondo Beach, CA,
H. Seiger, Waterford, CT
I. Servi, Kennecott Copper Corporation, Lexington, MA
R. C. Shair, Hollywood, FL
H. Shalit, ARCO Chemical Corp., Glenolden, PA
D. W. Sheibley, NASA-Lewis Research Center, Cleveland, OH
G. P. Smith, Oak Ridge National Laboratory, Oak Ridge, TN
J. Smits, Nevada Operations Office, DOE, Las Vegas, NV
F. Solomon, Electrode Media, Inc., Englewood, NJ
G. M. Thur, DOE, Office of Transportation Programs, Washington, DC
B. V. Tilak, Hooker Research Center, Grand Island, NY
L. Topper, National Science Foundation, Washington,
I. Trachtenberg, Texas Instruments, Dallas, TX
L. E. Vaaler, Battelle Columbus Laboratories, Columbus, OH
C. J. Venuto, C&D Batteries, Plymouth Meeting, PA

M. E. Wadsworth, U. of Utah, Salt Lake City, UT
R. D. Wherle, Sandia Labs, Albuquerque, NM
T. C. Wilder, Lexington, MA
M. E. Wilke, Burgess Battery Company., Freeport, IL
J. M. Williams, E. I. duPont de Nemours & Co., Wilmington, DE
E. Willihnganz, C&D Batteries, Plymouth Meeting, PA
J. F. Wing, Booz-Allen & Hamilton Inc., Bethesda, MD
J. C. Withers, Pora, Inc., Berea, OH
J. Wooldridge, Boeing Corp., Seattle, WA
V. Wouk, Petro-Electric Motor Ltd., New York, NY
L. Yanni, Booz-Allen & Hamilton Inc., Bethesda, MD
J. E. Zanks, NASA-Langley Research Center, Hampton, VA
M. Zlotnick, DOE, Conservation Research and Technology, Washington, DC
N. R. Bharucha, Noranda Research Center, Pointe Claire, Quebec, Canada
B. E. Conway, U. of Ottawa, Ontario, Canada
V. Ettel, INCO, Mississauga, Ontario, Canada
H. H. Horowitz, Alsthom-Exxon, Massy, France
N. Ibl, Technisch-Chemisches Laboratorium, Zurich, Switzerland
D. Landolt, Swiss Federal Institute of Technology, Lausanne, Switzerland